J Mater Sci: Mater Electron (2016) 27:11739–11750
DOI 10.1007/s10854-016-5312-9

Influence of deposition temperature on the optical, structural, morphological, compositional and photoelectrochemical properties of TiO_2 thin films

Neha D. Desai[1] · Sawanta S. Mali[2] · Rahul M. Mane[1] · Vishvanath B. Ghanwat[1] · Chang K. Hong[2] · Popatrao N. Bhosale[1]

Received: 18 March 2016 / Accepted: 4 July 2016 / Published online: 6 July 2016

Abstract In this investigation, we are reporting a photoelectrochemical (PEC) performance of TiO_2 thin films. Initially, TiO_2 thin films were synthesized by using a single step hydrothermal method. The influence of temperature on the optical, structural, morphological, compositional and PEC properties of TiO_2 thin films is investigated. The optical study reveals direct allowed type of transition. The XRD pattern confirms pure rutile phase with tetragonal crystal structure. The SEM analysis shows morphological transitions from 1D TiO_2 nanorods to give a 3D TiO_2 nanoflowers with increase in reaction temperature. The compositional data confirms the presence of titanium and oxygen in their respective oxidation state. HRTEM results confirm single crystalline nature of TiO_2 thin films. As the reaction temperature increased from 120 to 180 °C photoconversion efficiency is enhanced from 0.33 to 0.47 %. Along with PEC performance electrochemical impedance spectra of all the samples is measured.

1 Introduction

TiO_2 is one of the most important functional transition metal oxides (TMOs). It exhibits remarkable properties such as high chemical stability, high refractive index, low cost production, chemical and biological inertness etc. As a result of all these properties, TiO_2 is widely used for photocatalysis [1, 2], lithium ion batteries [3, 4], gas sensing [5], dye sensitized solar cells (DSSCs) [6] and so on.

There are number of methods for the synthesis of TiO_2 nanoparticles. Some of them are solvothermal [7], sol–gel [8], microwave assisted [9], electro spinning [10], hydrothermal [11] etc. Among all these synthesis techniques, hydrothermal method offers a promising approach for TiO_2 synthesis. Hydrothermal is a simple process as it offers a fast reaction kinetics as well as novel morphologies of TiO_2. Synthesis of hierarchical nanostructures with high surface area is possible with the hydrothermal method. The unique hierarchical structure provides novel physical and chemical properties for nanomaterials. The hydrothermal method also allows one to easily change the properties of materials such as crystallite size and morphology at nano level by simply changing the preparative parameters such as reaction temperature, precursor concentration, reaction time and pH. Thin film deposition by hydrothermal method involves the crystal growth of inorganic materials in the subcritical state of water. In this state, the physical and chemical properties of water like dielectric constant and viscosity changes substantially as compared to the normal water at normal temperature and pressure conditions [12]. Therefore, a change in temperature of hydrothermal method will alter the rate of precipitation of the metal ions indirectly affecting the growth rate of material under consideration. This change in growth rate affects the morphology as well as properties of nanomaterials.

There are number of approaches to fabricate TiO_2 nanorods, nanowires, nanofibres, nanoneedles, nanospheres including a nanoflower like morphology of TiO_2 [13–20]. Study of all these morphologies led to remarkable physicochemical properties. The preparation of TiO_2 nanomaterial with a controlled morphology is difficult task. In this regard, hydrothermal method provides a better opportunity to

✉ Popatrao N. Bhosale
p_n_bhosale@rediffmail.com

[1] Materials Research Laboratory, Department of Chemistry, Shivaji University, Kolhapur 416004, India

[2] School of Applied Chemical Engineering, Chonnam National University, Gwangju 500-757, South Korea

control over a size and morphology of TiO_2. Recently, Mali et al. [21] have reported a bottle brush like morphology for efficient DSSC applications. The Kim et al. [22] have also reported a hydrothermal synthesis of TiO_2 nanospheres.

Production of clean and renewable sources of energy by using a functional smart nanomaterials is the most challenging task. Thus researchers all over the world are now working on the photoelectrochemical (PEC) solar cells to obtain high photoconversion efficiency [23]. The hierarchical TiO_2 nanostructure are reported by Pawar et al. [24] with conversion efficiency of 0.13 %. Kong et al. [25] reported near about J_{sc} 100 μA/cm^2 for hierarchically structured mesoporous TiO_2 spheres synthesised using hydrolysis method. The Gao et al. [26] prepared by TiO_2 nanotube array membranes by potentistatic anodization having highest J_{sc} 110 μA/cm^2. Liu et al. [27] reported a TiO_2 nanorods by hydrothermal method. The well aligned TiO_2 nanorods prepared by hydrothermal method reported by Chen et al. [28]. All these aspects leads to the fact that TiO_2 is most suitable material to study PEC property.

In this investigation, we have studied the effect of deposition temperature on the optostructural, morphological, compositional properties of TiO_2 thin films synthesized via hydrothermal approach. Further the effect of deposition temperature on the PEC performance of TiO_2 film is also illustrated.

2 Experimental details

2.1 Materials and characterization

All the chemicals used for synthesis were of (AR) grade and used without further purification. Titanium tetraisopropoxide (TTIP; $C_{12}H_{28}O_4Ti$, 98 %, Spectrochem) was used as titanium precursor. Concentrated hydrochloric acid (HCl, 36 %, Thomas Baker) was used to maintain acidic condition of reaction solution. Fluorine doped tin oxide (FTO) coated on a glass substrates were used as for deposition of TiO_2 thin film. The FTO substrates were ultrasonically clean and finally rinsed with acetone.

The optical absorption spectra of TiO_2 thin films were recorded using UV–Vis–NIR spectrophotometer (Shimazdu UV-1800). The phase identification and crystal structure was determined by X-ray diffraction (XRD) technique (Bruker AXS D8 model). The (FT-IR) infrared spectroscopy was also used to confirm the TiO_2 phase. For this the TiO_2 samples were characterized by infrared spectrometer (Perkin Elmer, model 783 USA). The morphology and composition of all deposited thin films were studied by scanning electron microscopy (SEM) equipped with energy dispersive X-ray spectroscopic (EDS) analyser (JEOL-JSM 6360 A). The X-ray photoelectron spectroscopy (XPS) analysis was carried out on (VG Multilab 2000) instrument. The high resolution transmission electron microscopy (HRTEM) analysis with selected area electron diffraction (SAED) pattern was carried out on TECHNAI Phillip F20 microscope. The J–V characteristic curve was recorded using a linear sweep voltametry using (Autolab PGSTAT 100 potentiostat).

2.2 Solar cell fabrication

The PEC measurement was carried out by irradiating the TiO_2 photoanode with UV light recorded at electrochemical workstation AUTOLAB PGSTAT100 potentiostat. The PEC cell was a two electrode system, TiO_2 is a working electrode with active surface area of 1 cm^2, Graphite as a counter electrode and 0.1 M NaOH was used as an electrolyte illuminated by 5 mW/cm^2 intensity UV source [29].

Further the electrochemical impedance spectroscopy (EIS) measurement was also carried out on the same instrument with a standard 3 electrode system. Platinum as counter electrode, TiO_2 as working electrode and Ag/AgCl as reference electrode. 0.1 N NaOH was used as electrolyte for EIS measurement.

2.3 Deposition of TiO_2 thin films

The TiO_2 thin films are deposited by using a simple hydrothermal method. In a typical synthesis of TiO_2, equal volume of distilled water and conc. HCl are taken. To this solution 0.5 mL of TTIP solution is added. The whole solution was stirred using a magnetic stirrer for 30 min. After that the clear and transparent solution was poured in a Teflon lined autoclave with 25 mL capacity. Then the FTO conducting substrate is immersed into the solution inclined to the wall with conducting side facing up. The autoclave was sealed and placed in an oven at 120 °C for 3 h having air atmosphere. This obtained TiO_2 sample was designated as T_{12}. Using the same experimental procedure samples were deposited at 140, 160 and 180 °C deposition temperature and designated as T_{14}, T_{16} and T_{18} respectively. After cooling the autoclave at room temperature, TiO_2 thin films were taken out of it. The films were washed for several times with deionized water and dried in oven for 1 h at 100 °C. Further films were annealed for 1 h at 400 °C in muffle furnace. Preparative parameters for the deposition of TiO_2 thin films are given in Table 1.

3 Results and discussion

3.1 Possible growth and reaction mechanism

In the present study, reaction time is 3 h which is kept constant for all the samples and deposition temperature is

Table 1 Optimized preparative parameters for TiO_2 thin film deposition

Sample code	Bath composition	Deposition temperature (°C)	Deposition time (h)
T_{12}	0.5 mL TTIP + equal volume of distilled water and Conc. HCl	120	3
T_{14}		140	
T_{16}		160	
T_{18}		180	

varied from 120 to 180 °C. The influence of deposition temperature on the properties of desired material plays a crucial role in the growth mechanism. The thin film formation by hydrothermal method substantially changes the physical and chemical properties of water. The change in temperature in hydrothermal method affects the crystal growth. The change in deposition temperature results in the change in growth rate. The change in the growth rate affects the morphology of nanomaterial [30]. As a result of this morphological transitions from initially grown TiO_2 nanorods to fully grown TiO_2 nanoflowers is observed as a function of deposition temperature. This morphological evolution is shown in the Fig. 1. Here titanium tetra isopropoxide is used as Ti precursor. The TiO_2 thin film formation follows a heterogeneous nucleation. The heterogeneous nucleation is achieved by low degrees of supersatuation. The acidic conditions are required for the low degrees of supersaturation. To maintain the acidic conditions conc. HCl is used in this typical synthesis. The chemical reactions involved in this typical synthesis are as follows, Initially, TTIP reacts with the water to form a titanium hydroxide $Ti(OH)_4$ in the hydrolysis reactions. This $Ti(OH)_4$ forms a TiO_2 and water molecule is removed during the process of condensation.

$$Ti(OR)_4 + 4H_2O \rightarrow Ti(OH)_4 + 4ROH \text{ (hydrolysis)}$$
$$Ti(OH)_4 \rightarrow TiO_2 + 2H_2O \text{ (condensation)}$$

The morphology varies with the temperature. Initially at 120 °C there is formation of TiO_2 nanorods. With increase in temperature number of nanorods assembled to form a bunch of nanorods. The nanorods are aggregated with further increase in temperature and finally fully grown nanoflowers of TiO_2 is obtained.

3.2 Optical study

The UV–visible absorption spectra of all TiO_2 samples i.e. T_{12}–T_{18} was recorded in the range of 200–1100 nm. It is shown in Fig. 2. The fundamental absorption edge in most semiconductors follow the exponential law. Using the absorption data, the band gap was estimated by Tauc's relation [31],

$$\alpha h\nu = A\,(h\nu - E_g)^n \quad (1)$$

where α is absorption coefficient, $h\nu$ is photon energy, E_g is optical band gap, n depends on the type of electronic transition. The energy gap of TiO_2 thin films is determined by extrapolating the linear portion of the plots of $(\alpha h\nu)^2$ versus $h\nu$ to the energy axis. The observed band gap energy for samples T_{12}, T_{14}, T_{16} and T_{18} is 3.36, 3.29, 3.18 and 3.15 eV respectively. The highest value of a band gap is observed for sample T_{12} for which deposition temperature is 120 °C and lowest value is observed for sample T_{18} for which deposition temperature is 180 °C. So it can be observed that with increase in the deposition temperature, band gap of TiO_2 thin film is decreased. The band gap of the material can also be co-related with the morphologies of TiO_2 thin films. The lowest band gap is observed for sample T_{18} which shows nanoflower like morphology on the other hand nanorods like morphology of sample T_{12} shows highest band gap. All the samples of TiO_2 thin films show direct allowed type of transition. The tuning of a band gap with morphological modification is beneficial for

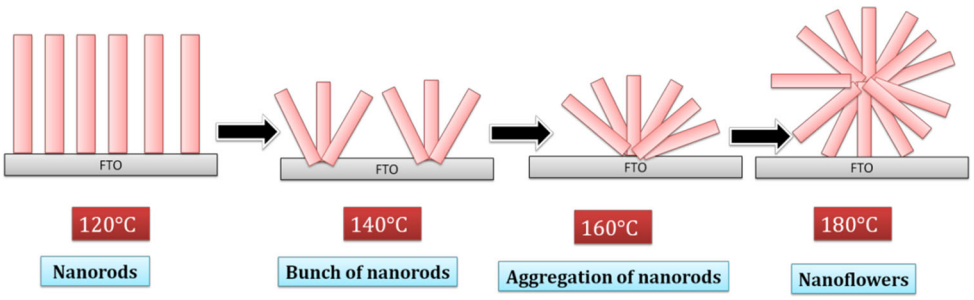

Fig. 1 Graphical mechanism of TiO_2 thin film formation

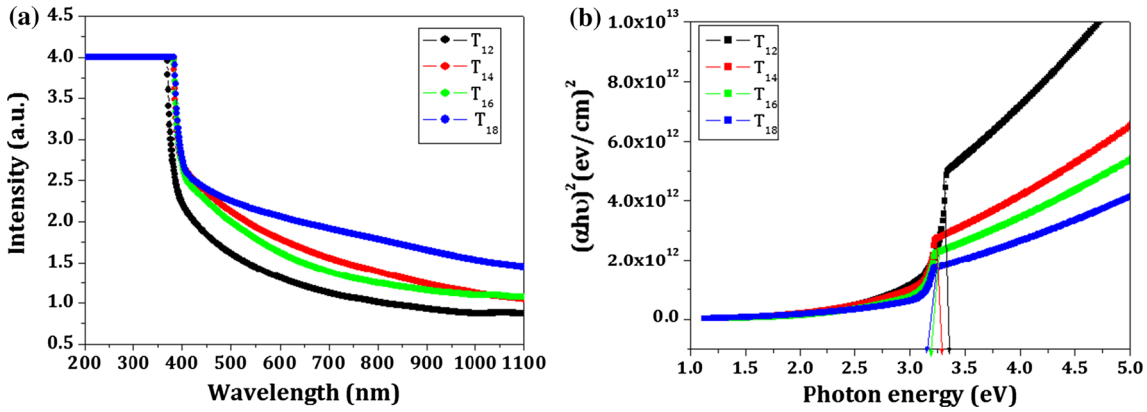

Fig. 2 **a** Absorption spectrum and **b** optical band gap of TiO_2 thin films

the maximum absorption of light in the visible region of solar spectrum.

3.3 Structural study

The crystal structure and crystallite size of TiO_2 thin films was determined by (XRD) pattern. Figure 3 shows XRD pattern of sample T_{12}–T_{18} deposited at different reaction temperature. All the peaks in the XRD pattern are well indexed to the JCPDS card no. 21-1276 confirming the pure rutile phase formation with a tetragonal crystal structure [32]. The XRD peaks are observed at 27.46°, 36.18°,41.43°, 54.36°,56.46°, 62.87° and 69.91° designated

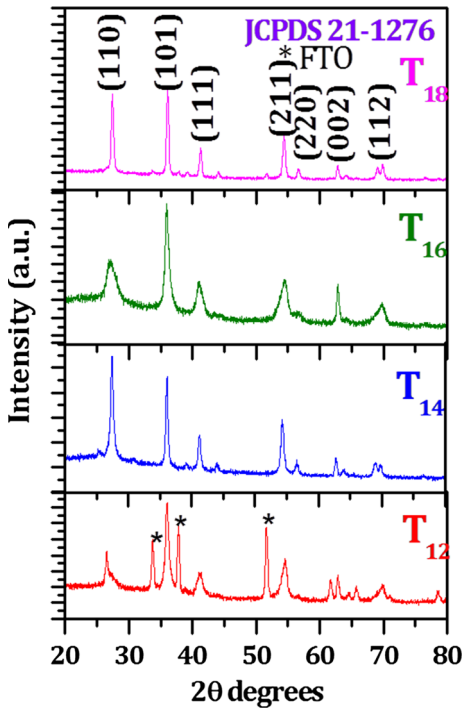

Fig. 3 XRD pattern of TiO_2 thin films

to (110), (101), (111), (211), (220), (002) and (112) planes respectively. All the peaks are well assigned to the rutile phase. No extra peaks due to impurity are observed. The crystallite size was calculated by using well known Debye–Scherer equation. The calculated values for crystallite size are 67, 33, 31 and 22 nm for T_{12}, T_{14}, T_{16} and T_{18} respectively. The microstrain (ε) was calculated by using the Eq. (2),

$$\varepsilon = \frac{\beta \cos\theta}{4} \tag{2}$$

Further the lattice parameters are also calculated by the following Eq. (3),

$$\frac{1}{d^2} = \frac{h^2 + k^2}{a^2} + \frac{l^2}{c^2} \tag{3}$$

The calculated values for 'a' and 'c' are a = 4.56 and c = 2.93 Å. These values are in good agreement with standard values mentioned in JCPDS card 21-1276. This confirms the formation of tetragonal crystal structure. All the results from XRD analysis are given in the Table 2.

Here, the most intense peaks is associated with (110) plane. As the deposition temperature increases intensity of (101) plane also increases. The crystallite size decreases with increase in the deposition temperature. This means that higher is the deposition temperature, smaller is the crystallite size.

Further with increase in the crystallite size, value of microstrain increases. Improvement in crystallinity results in decrease in lattice defects. This indicates that TiO_2 is highly crystalline.

3.4 FT-IR analysis

The FT-IR spectra for all the samples T_{12} to T_{18} are recorded in the frequency range of 500–4000 cm^{-1}. The FT-IR spectrum is shown in Fig. 4. The band at 673 cm^{-1} is due to the titanium dioxide and assigned to the Ti–O–Ti

Table 2 Values for crystallite size (D), microstrain (ε) of TiO_2

Sample code	D (nm)	$\varepsilon \times 10^{-3}$ (n/m^2)
T_{12}	67	5.14
T_{14}	33	1.05
T_{16}	31	1.10
T_{18}	22	1.53

stretching. The peak centred at 1019 cm^{-1} is because of characteristic O–O stretching vibrations. The absorption band at 1632 cm^{-1} is due the bending vibration of co-ordinated H_2O as well as Ti–OH. The wide peak observed at 3100–3600 cm^{-1} is attributed to the presence of hydroxyl groups. All these facts confirms the TiO_2 formation [33].

3.5 Morphological study

In order to study morphology of TiO_2 thin films deposited at different deposition temperature, SEM analysis was performed. The low and high resolution SEM images are shown in the Fig. 5 [34]. The morphological evolution from nanorods to nanoflowers is observed as a function of temperature. All SEM images show well adherent, pinhole free thin film formation.

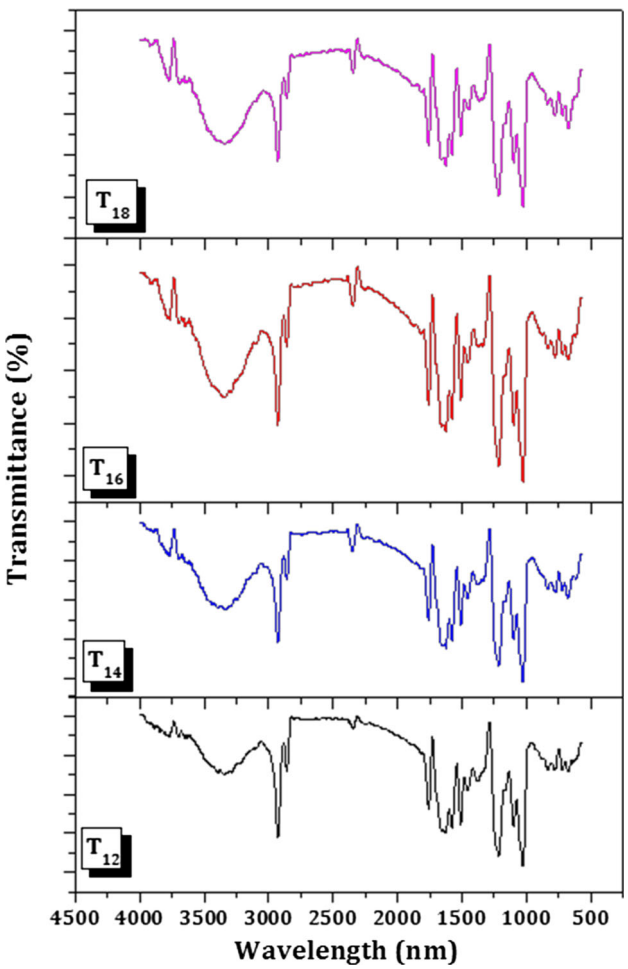

Fig. 4 FT-IR of TiO_2 thin films

There is a formation of a well grown 3D nanoflowers on the FTO substrate. This formation exhibits a step by step growth mechanism. In case of sample T_{12}, initially there is a formation of a well aligned 1D TiO_2 nanorods. After increasing the reaction temperature to 140 °C (sample T_{14}) presents the formation of bunch of nanorods. The high magnification images shows that nanorods forms bunches and connects with a one root to form a 3D nanoflowers. The nanoflower provides a large active surface area and higher absorption of incident photons. This results in the generation of electron–hole pair. The recombination of electron–hole pair causes a higher photoconversion efficiency.

As temperature shifts to 160 °C, number nanoflowers are aggregated to form a compact densely packed 3D nanoflower like structure. When the temperature is 180 °C, then perfect nanoflower like morphology with sharpen edges is obtained. This fact indicates that temperature plays an important role in the morphology. The morphology evolution from nanorods to nanoflowers is a temperature dependent phenomenon. Further this morphological transition can be also co-related with XRD study. The most intense (110) plane is responsible for the anisotropic growth of nanomaterials. So there is a tendency of (110) plane to favour the growth of flower like structure As the temperature increases intensity of (110) plane also increases [35]. Hence there is a formation of nanoflower like morphology with increase in the temperature. Thus, in a nutshell, we are reporting here 1D nanorods as well as 3D nanoflowers in the present study. Both of these morphologies are beneficial for PEC performance.

To study details of crystallinity we have also carried, HRTEM analysis along with selected area electron diffraction (SAED) pattern are shown in the Fig. 6. The HRTEM images clearly shows presence of nanorod which is in agreement with SEM results. Each nanorod has a tetragonal facet. It can be observed that number of nanorods are combining on a same root to give flower like morphology of TiO_2. Each nanorod has a length of about 400 nm and width of about 100 nm. This can be observed from Fig. 5c. Each nanorods is formed by the aggregation of number of TiO_2 nanoparticles with a tetragonal facets. The lattice fringes are also clearly observed in HR-TEM. The SAED pattern of TiO_2 thin film shows a bright dotted pattern. The bright spots confirms the single crystalline nature of TiO_2 [36]. SAED pattern reveals that TiO_2 nanoflowers is not aggregation of small crystallites but it is made up of monocrytals nanorods growing homocentrically confirming the single crystalline nature of TiO_2 thin

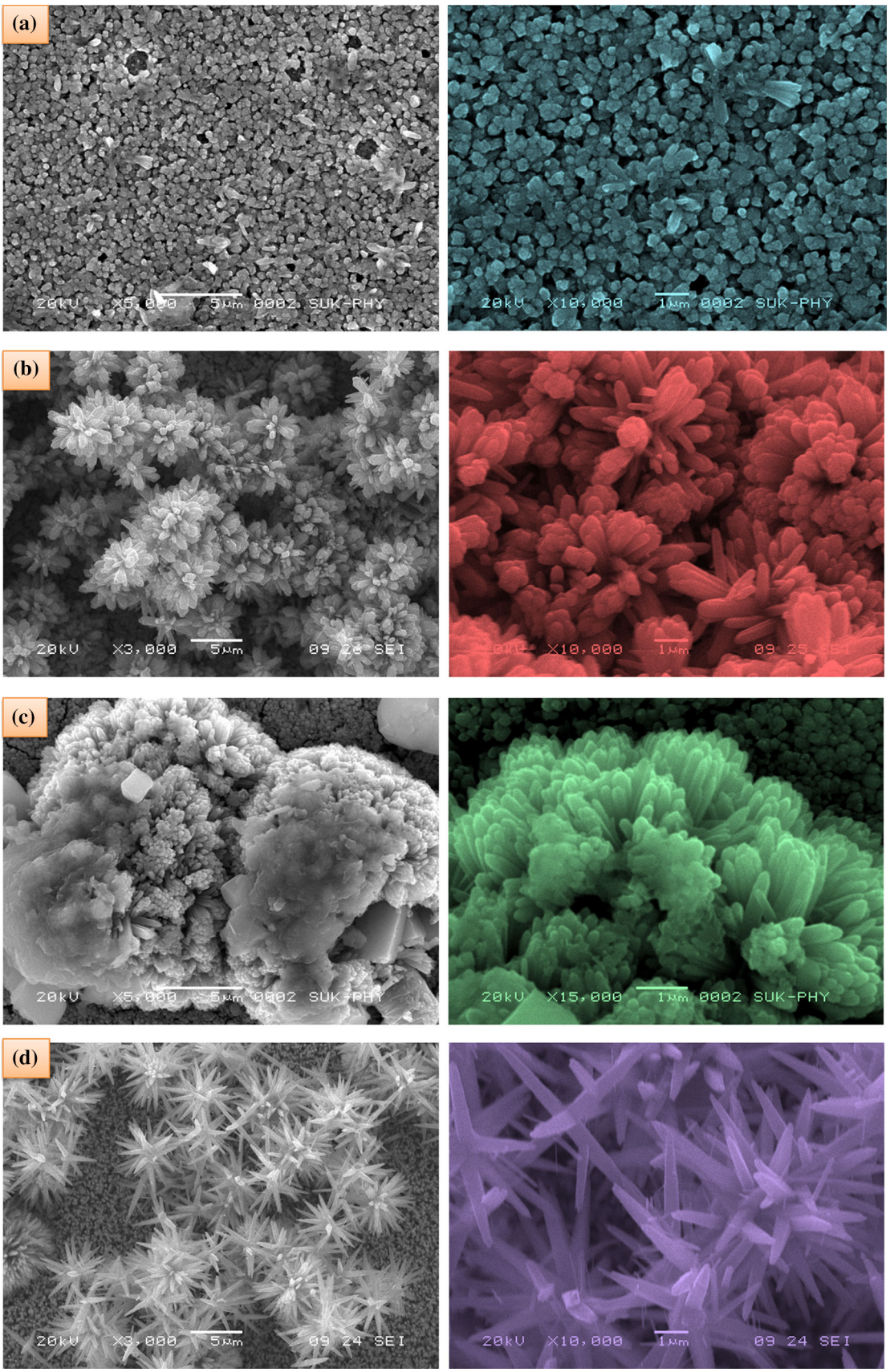
(a)
20kV X5,000 5μm 0002 SUK-PHY
20kV X10,000 1μm 0002 SUK-PHY
(b)
20kV X3,000 5μm 09 Z5 SEI
20kV X10,000 1μm 09 Z5 SEI
(c)
20kV X5,000 5μm 0002 SUK-PHY
20kV X15,000 1μm 0002 SUK-PHY
(d)
20kV X3,000 5μm 09 24 SEI
20kV X10,000 1μm 09 24 SEI

◀**Fig. 5** SEM images of TiO_2 thin film **a** sample T_{12}, **b** sample T_{14}, **c** sample T_{16}, **d** sample T_{18}

films. All these results obtained from HRTEM analysis are in well agreement with SEM results.

3.6 Compositional study

The quantitative analysis of all the four samples T_{12}, T_{14}, T_{16} and T_{18} was carried out using EDS analysis. The EDS spectra of all sample is shown in Fig. 7. The presence of titanium and oxygen in all the samples was confirmed by EDS. The expected atomic percentage for titanium and oxygen is 20 and 80 % respectively. The observed atomic percentage for both the elements is in good agreement with expected atomic percentage. The EDS spectra of TiO_2 sample shows 2 peaks at 4.48 and 0.50 eV for the presence of titanium and oxygen. There is no trace of any other impurities within the detection limit of EDS.

XPS analysis was carried out to determine the chemical composition and oxidation states of titanium and oxygen present in the TiO_2 thin film. The Fig. 8 shows a XPS survey spectrum of TiO_2. This confirms the presence of titanium, oxygen along with the small amount of adventitious carbon. The presence of carbon in XPS analysis is due to residual carbon from XPS instrument itself. It shows a core level spectrum of Ti2*p* with a spin orbit doublets as $Ti2p_{3/2}$ and $Ti2p_{1/2}$ observed at 458.40 and 464.22 eV respectively. It also shows a singlet peak of O1*s* observed at binding energy 529.71 eV confirming presence of oxygen. +4 and −2 oxidation states for titanium and oxygen is also confirmed from XPS analysis [37].

3.7 Photoelectrochemical performance of TiO_2 thin films

The J–V characteristic properties of TiO_2 thin films was recorded using a linear sweep voltametry as shown in Fig. 9. Here TiO_2 thin films acts as working electrode and

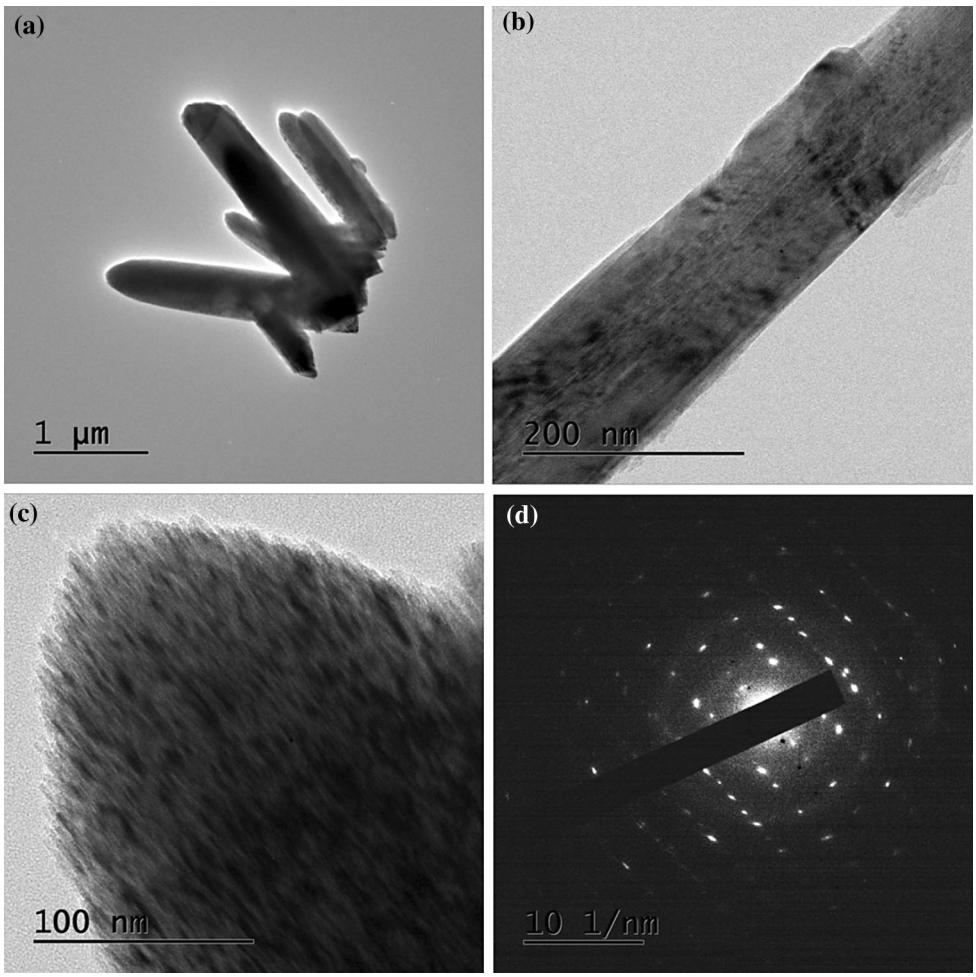

Fig. 6 **a–c** HRTEM and **d** SAED pattern of representative T_{14} sample

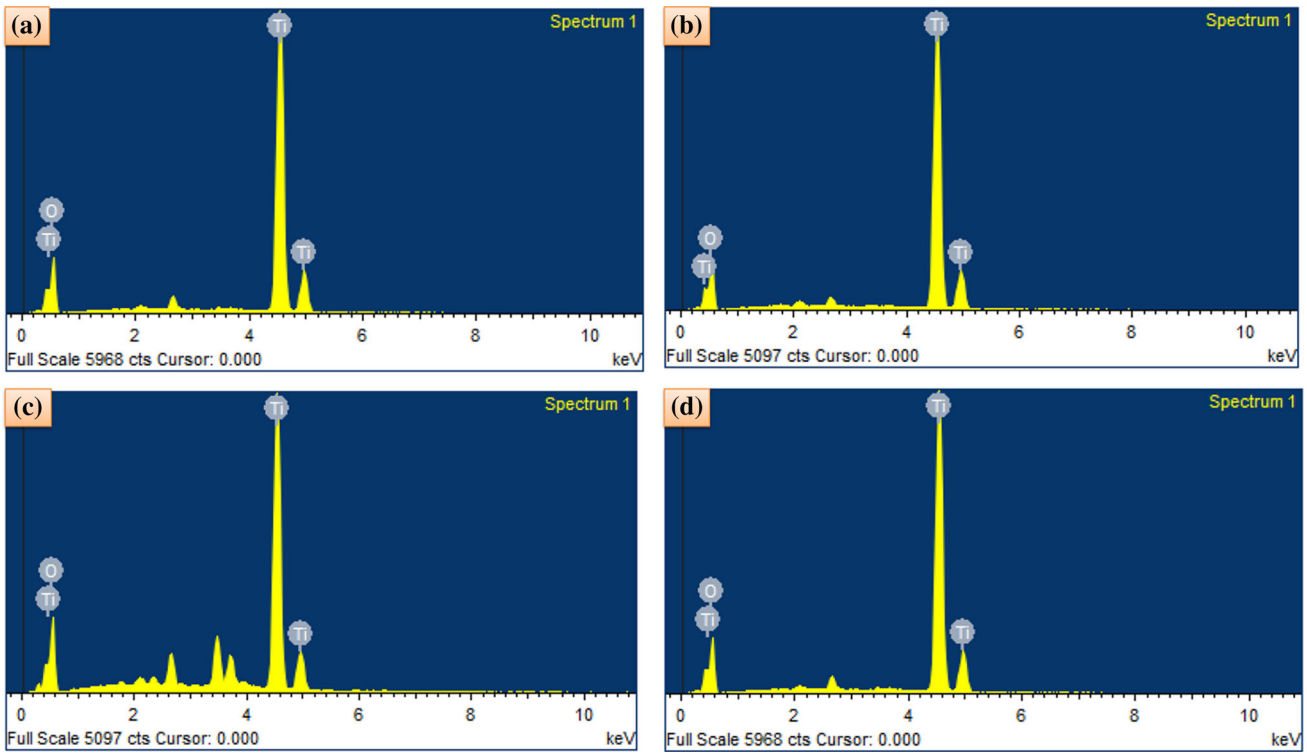

Fig. 7 EDS spectrum of TiO_2 thin film **a** sample T_{12}, **b** sample T_{14}, **c** sample T_{16}, **d** sample T_{18}

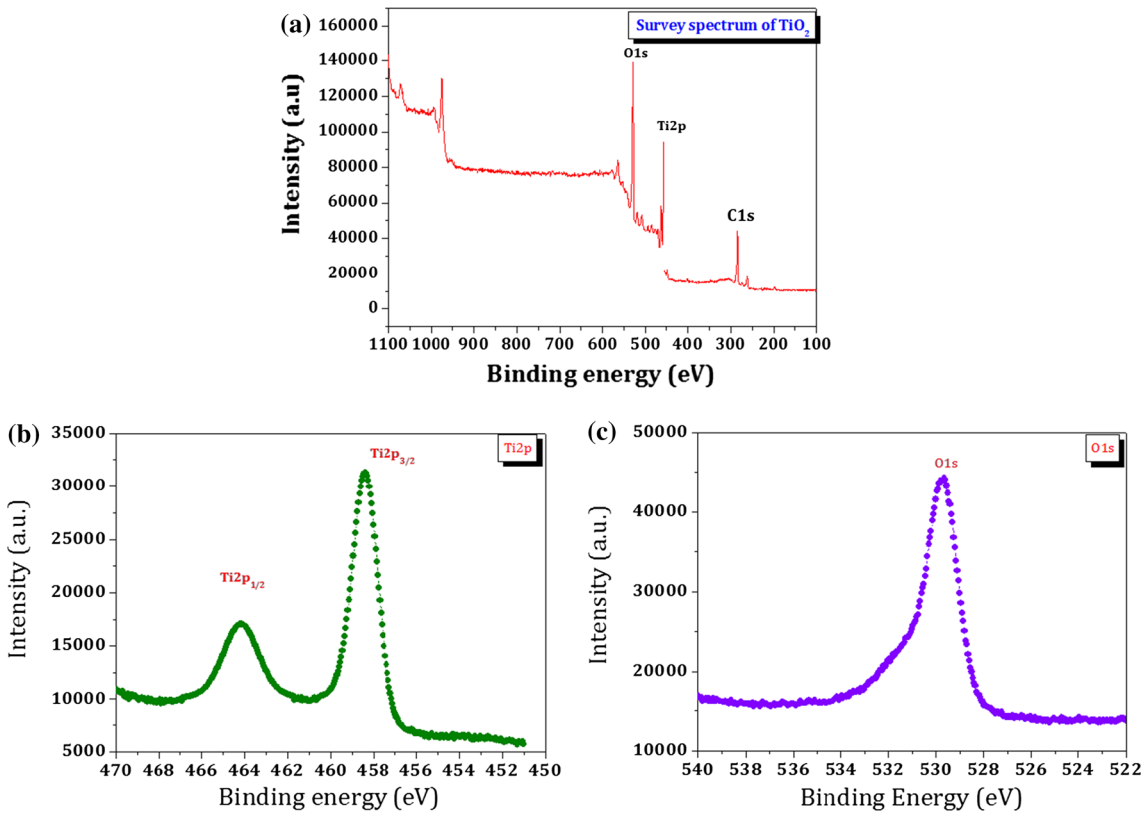

Fig. 8 XPS analysis of TiO_2 **a** survey spectrum of TiO_2, **b** core level spectrum of Ti2*p* and **c** core level spectrum of O1*s* for representative sample T_{14}

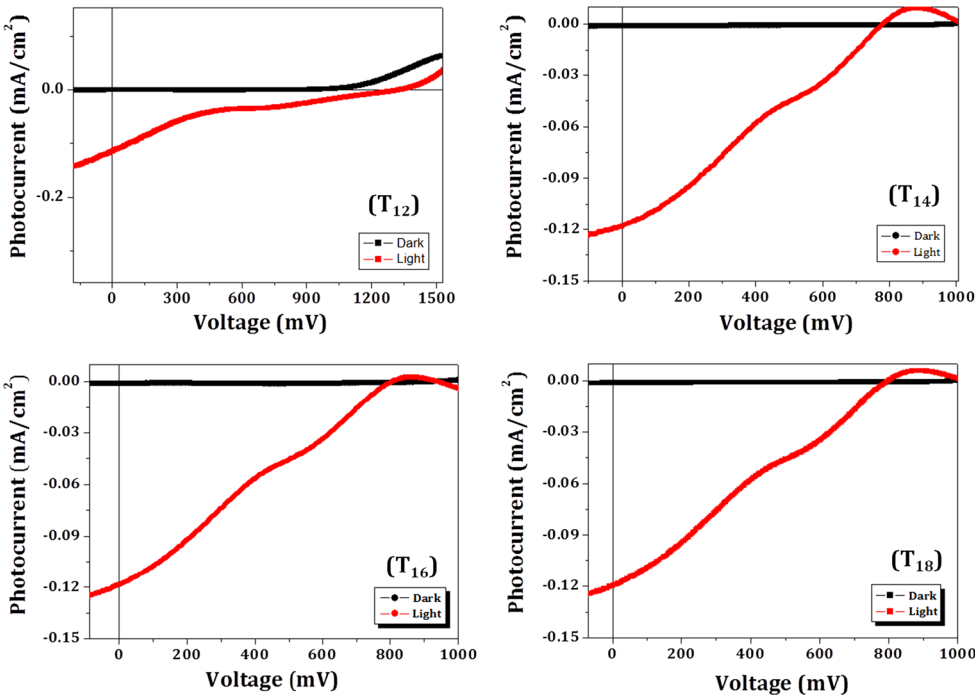

Fig. 9 J–V curves of all TiO_2 thin films

graphite as a counter electrode. The 0.1 M NaOH is used as redox electrolyte. The UV lamp with a power 5 mW/cm^2 is used as a source of illumination. The following cell configuration is used for PEC measurements.

FTO/TiO_2/0.1N NaOH/Graphite

The photoelectrode shows an ideal diode like rectifying characteristics in a dark. The solar cell parameters such as FF and η% are calculated by using given Eqs. (4) and (5) [38],

$$\mathrm{FF} = \frac{\mathrm{Jmax} \times \mathrm{Vmax}}{\mathrm{J}sc \times Voc} \tag{4}$$

$$\eta\,\% = \frac{\mathrm{Jsc} \times Voc}{\mathrm{Pin}} \times \mathrm{FF} \times 100 \tag{5}$$

where J_{sc} is the short circuit current density, V_{oc} is the open circuit voltage, J_{max} is the maximum current density, V_{max} is the maximum voltage and P_{in} is the input light intensity. The obtained values of J_{sc} for sample T_{12}, T_{14}, T_{16}, T_{18} were 0.1139, 0.1169, 0.1175 and 0.1192 mA/cm^2 respectively. The corresponding values of V_{oc} are 1216, 778, 790 and 788 mV respectively. It was found that as the reaction temperature increases from 120 to 180 °C photoconversion efficiency increases from 0.33 to 0.47 %. All obtained PEC parameters are given in Table 3.

In case of sample T_{12}, the light is directly transferred through 1D nanorods without scattering results in low photoconversion efficiency (0.33 %). While as the reaction temperature is proceed to 140 °C, the conversion efficiency increased and reaches to 0.43 %. The TiO_2 photoanode can absorb enough amount of light to generate electron hole pair. The transfer of electrons from filled valence band to empty conduction band occurs. The photogenerated electrons can transport through crystallites and compact layers with minimum loss. The photogenerated electrons travel through external load and completes the circuit by entering back through counter electrode.

The improvement in the photoconversion efficiency is explained on the basis of surface modification by reaction temperature. The TiO_2 is formed by a two step structure. 3D nanoflower like structure acts as overlayer and 1D nanorods acts like underlayer. The 1D nanorods can

Table 3 PEC cell parameters of TiO_2 thin films

Sample	J_{sc} (mA/cm^2)	V_{oc} (mV)	J_{max} (mA/cm^2)	V_{max} (mV)	FF	η%
T_{12}	0.1139	1216	0.044	408.04	0.12	0.33
T_{14}	0.1169	778	0.050	438.65	0.24	0.43
T_{16}	0.1175	790	0.047	478.80	0.24	0.44
T_{18}	**0.1192**	**788**	**0.058**	**407.09**	**0.25**	**0.47**

Bold values indicate the highest photoconversion efficiency which is shown by sample T_{18}

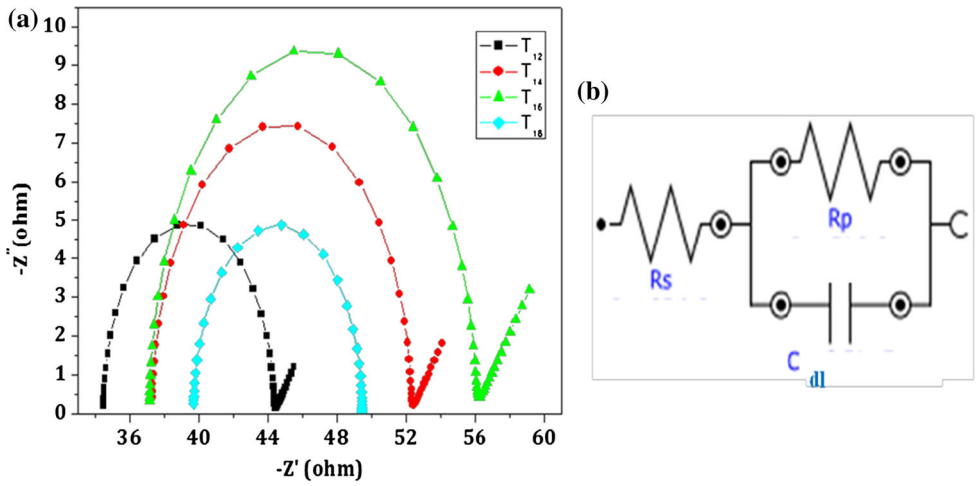

Fig. 10 **a** Nyquist plot for and **b** equivalent circuit of EIS for T_{12}–T_{18} samples

accelerate the movement of electrons in one direction. While 3D flower like structure provides a higher surface area. The effective scattering of light is possible in 3D structures. The scattering of light in 3D structure enhances PEC performance.

3.8 EIS measurement study

The electrochemical impedance is a powerful technique used to measure the ability of a circuit to resists the flow of electric current. EIS is a well known technique for the determination of a charge transport and recombination mechanism. The Fig. 10a shows a Nyquist plots of EIS spectra of TiO_2 thin films deposited at different reaction temperature. The electrochemical impedance measurements were carried out by applying a open circuit voltage in a dark conditions recorded over a frequency range of 30–60 kHz. The corresponding simplified equivalent circuit is given in Fig. 10b.

The Nyquist plot is composed of semicircle with a sloping line. The higher and middle frequency region forms a semicircle while a sloping line indicates a lower frequency region [39, 40]. All the EIS parameters are shown in the Table 4.

R_s is the series resistance related to the transport resistance of the FTO substrates. R_p is the charge transfer resistance at the counter electrode/electrolyte interface corresponding to the smaller semicircle. C_{dl} is the charge transfer resistance between TiO_2/electrolyte interface corresponding to larger semicircle. The larger semicircle indicates a slow charge recombination rate. Thus a lowest value of C_{dl} i.e. charge transfer resistance provides a optimum photoconversion efficiency.

The sample T_{18} shows a smallest value of C_{dl}. In addition to this, lower value of C_{dl} means low charge transfer resistance. This leads to the high network of photogenerated electrons. All these facts are leading to the better photoconversion efficiency. Hence all PEC results are supported by EIS measurement.

Table 4 EIS parameters of TiO_2 thin films

Sample	R_s Ω	R_p Ω	C_{dl}
T_{12}	34.5	9.85	7.20
T_{14}	35.7	9.77	6.12
T_{16}	37.2	18.8	4.92
T_{18}	37.3	15	3.63

4 Conclusions

In this study, hierarchical TiO_2 nanostructures are obtained by a simple single step hydrothermal method. The effect of deposition temperature on the optical, structural, morphological, compositional and PEC performance of TiO_2 thin films have been investigated. The present study indicates that deposition temperature plays a crucial role in the morphology as well as PEC performance. The formation of 1D nanorods assembled to form 3D TiO_2 nanoflowers contribute positively in the photoconversion efficiency. The morphological study manifests that 3D nanoflower act as a scattering layer for light while 1D nanorods acts as underlayer. The increase deposition temperature (120–180 °C) results in the increase in the PEC performance (0.33–0.47 %). This increase in the efficiency is due to less resistance to electron transfer and reduction in charge recombination rate. Overall study signifies that deposition temperature plays a key role in the optoelectronic properties of TiO_2 thin films.

Acknowledgments One of the authors Miss. Neha Desai is very much thankful to Department of Science and Technology (DST), New Delhi for awarding DST-INSPIRE Fellowship (IF 140575). This work

is also supported by Basic science research programme through the National Science Research Foundation of Korea (NRF) funded by Ministry of education (NRF-2009-0094055).

References

1. S.M. Gupta, M. Tripathi, A review of TiO_2 nanoparticles. Chin. Sci. Bull. **56**, 1639–1657 (2011)
2. M.A. Henderson, A surface science perspective on TiO_2 photocatalysis. Surf. Sci. Rep. **66**, 185–297 (2011)
3. V. Aravindan, Y. Lee, R. Yazami, S. Madhavi, TiO_2 polymorphs in rocking chair Li-ion batteries. Mater. Today **18**, 345–351 (2015)
4. B.L. Sypien, M. Radecka, M. Rekas, K. Swierczek, K. Mauke, T. Graule, K. Zakrzewska, Grain-size-dependent gas-sensing properties of TiO_2 nanomaterials. Sens. Actuators B Chem. **211**, 67–76 (2015)
5. Y. Fan, H. Lu, J. Liu, C. Yang, Q. Jing, Y. Zhang, X. Yanga, K. Huanga, Hydrothermal preparation and electrochemical sensing properties of TiO_2–graphene nanocomposite. Colloids Surf. B **83**, 78–82 (2011)
6. A. Tale, F. Mesguich, A. Hérissan, C. Colbeau-Justin, X. Yanpeng, P. Dubot, Optimized TiO_2 nanoparticle packing for DSSC photovoltaic applications. Sol. Energy Mater. Sol. Cells **148**, 52–59 (2016)
7. Y. Gonseo, M. Kim, H. Lee, W. Lee, Solution processed thin films of non-aggregated TiO_2 nanoparticles prepared by mild solvothermal treatment. Sol. Energy Mater. Sol. Cells **95**, 332–335 (2011)
8. V. Zunic, M. Vukomanović, S.D. Škapin, D. Suvorov, J. Kovac, Photocatalytic properties of TiO_2 and TiO_2/Pt: a sol-precipitation, sonochemical and hydrothermal approach. Ultrason. Sonochem. **21**, 367–375 (2014)
9. L. Mao, Y. Wang, Y. Zhong, J. Ning, Y. Hu, Microwave-assisted deposition of metal sulfide/oxide nanocrystals onto a 3D hierarchical flower-like TiO_2 nanostructure with improved photocatalytic activity. J. Mater. Chem. A **1**, 8101–8104 (2013)
10. D. Vernardou, E. Stratakis, G. Kenanakis, H. Yates, S. Courish, M. Pemblej, E. Koudoumas, N. Katsarakis, One pot direct hydrothermal growth of photoactive TiO_2 films on glass. J. Photochem. Photobiol. **202**, 81–85 (2009)
11. A. Hosseini, K. Icli, M. Ozenbra, C. Ercelebi, Fabrication and characterization of spin-coated TiO_2 films. Energy Procedia **60**, 191–198 (2014)
12. W. Shi, S. Song, H. Zhang, Hydrothermal synthetic strategies of inorganic semiconducting nanostructures. Chem. Soc. Rev. **42**, 5714–5743 (2013)
13. Y. Kim, P. Rai, Y. Yu, Microwave assisted hydrothermal synthesis of Au@TiO_2 core–shell nanoparticles for high temperature CO sensing applications. Sens. Actuators B Chem. **186**, 633–639 (2013)
14. N. Rahmani, R.S. Dariania, M. Rajabi, A proposed mechanism for investigating the effect of porous silicon buffer layer on TiO_2 nanorods growth. Appl. Surf. Sci. **366**, 359–364 (2016)
15. Y. Tang, L. Hong, Q. Wu, J. Li, G. Hou, H. Cao, L. Wu, G. Zheng, TiO_2(B) nanowire arrays on Ti foil substrate as three-dimensional anode for lithium-ion batteries. Electrochim. Acta **195**, 27–33 (2016)
16. W. Jung, N. Kwak, T. Hwang, K. Yi, Preparation of highly porous TiO_2 nanofibers for dye-sensitized solar cells (DSSCs) by electro-spinning. Appl. Surf. Sci. **261**, 343–352 (2012)
17. R.A. Patil, R.S. Devan, Y. Liou, Y. Ma, Efficient electrochromic smart windows of one-dimensional pure brookite TiO_2 nanoneedles. Sol. Energy Mater. Sol. Cells **147**, 240–245 (2016)
18. T. Kasuga, M. Hiramatsu, A. Hoson, T. Sekino, K. Niihara, Formation of titanium oxide nanotube. Langmuir **14**, 3160–3163 (1998)
19. Q. Zhang, W. Li, S. Liu, Controlled fabrication of nanosized TiO_2 hollow sphere particles via acid catalytic hydrolysis/hydrothermal treatment. Powder Technol. **212**, 145–150 (2011)
20. A.A. Umar, M.Y.A. Rahman, S.K.M. Saad, M.M. Salleh, M. Oyama, Preparation of grass-like TiO_2 nanostructure thin films: effect of growth temperature. Appl. Surf. Sci. **270**, 109–114 (2013)
21. S.S. Mali, J.V. Patil, P.M. Kadam, H.P. Deshmukh, C. Shim, P.S. Patil, C.K. Hong, Hydrothermal synthesis of rutile TiO_2 bottle brush for efficient dye-sensitized solar cells. J. Nanopart. Res. **16**, 2406–2416 (2014)
22. Y.J. Kim, M.H. Lee, H.J. Kim, G. Kim, Y.S. Choi, N.G. Park, K. Kim, W.I. Lee, Formation of highly efficient dye-sensitized solar cells by hierarchical pore generation with nanoporous TiO_2 spheres. Adv. Mater. **21**, 3668–3673 (2009)
23. V.V. Kondalkar, S.S. Mali, N.B. Pawar, R.M. Mane, S. Choudhury, C.K. Hong, P.S. Patil, S.R. Patil, P.N. Bhosale, J.H. Kim, Microwave-assisted rapid synthesis of highly porous TiO_2 thin films with nanocrystalline framework for efficient photoelectrochemical conversion. Electrochim. Acta **143**, 89–97 (2014)
24. S.A. Pawar, R.S. Devan, D.S. Patil, V.V. Burungale, T.S. Bhat, S.S. Mali, S.W. Shin, J.E. Ae, C.K. Hong, Y.R. Ma, J.H. Kim, P.S. Patil, Hydrothermal growth of photoelectrochemically active titanium dioxide cauliflower-like nanostructures. Electrochim. Acta **117**, 470–479 (2014)
25. E.H. Kong, Y.J. Chang, H.M. Jang, Quantum dot-sensitized mesoporous spherical TiO_2 paste with cyclic calcination for photoelectrochemical cells. Electrochim. Acta **132**, 98–102 (2014)
26. S. Gao, J. Yang, M. Liu, H. Yan, W. Li, J. Zhang, Y. Luo, Enhanced photovoltaic performance of CdS quantum dots sensitized highly oriented two-end-opened TiO_2 nanotubes array membrane. J. Power Sources **250**, 174–180 (2014)
27. B. Liua, D. Wanga, L. Wang, Y. Suna, Y. Lina, X. Zhanga, T. Xie, Glutathione-assisted hydrothermal synthesis of CdS-decorated TiO_2 nanorod arrays for quantum dot-sensitized solar cells. Electrochim. Acta **113**, 661–667 (2013)
28. Y. Chen, Q. Tao, W. Fu, H. Yang, X. Zhou, S. Su, D. Ding, Y. Mu, X. Li, M. Li, Enhanced photoelectric performance of PbS/CdS quantum dots co-sensitized solar cells via hydrogenated TiO_2 nanorod arrays. Chem. Commun. **50**, 9509–9512 (2014)
29. A. Sobhani-Nasab, M. Rangraz-Jeddy, A. Avanes, M. Salavati-Niasari, Novel sol–gel method for synthesis of $PbTiO_3$ and its light harvesting applications. J. Mater. Sci.: Mater. Electron. **26**, 9552–9560 (2015)
30. P.B. Patil, S.S. Mali, V.V. Kondalkar, K.V. Khot, R.M. Mane, C.K. Hong, P.S. Patil, J.H. Kim, P.N. Bhosale, An approach towards TiO_2 chrysanthemum flowers with tunable properties: influence of reaction time in hydrothermal process. J. Mater. Sci.: Mater. Electron. **26**, 6119–6128 (2015)
31. S. Mostafa Hosseinpour-Mashkani, A. Sobhani-Nasab, A simple sonochemical synthesis and characterization of $CdWO_4$ nanoparticles and its photocatalytic application. J. Mater. Sci.: Mater. Electron. **27**, 3240–3244 (2016)
32. T. Ohno, K. Sarukawa, M. Matsumura, Crystal faces of rutile and anatase TiO_2 particles and their roles in photocatalytic reactions New. J. Chem. **26**, 1167–1170 (2002)
33. S.S. Mali, P.S. Shinde, C.A. Betty, P.N. Bhosale, W.J. Lee, P.S. Patil, Nanocoral architecture of TiO_2 by hydrothermal process: synthesis and characterization. Appl. Surf. Sci. **257**, 9737–9746 (2011)
34. A. Sobhani-Nasab, S. Mostafa Hosseinpour-Mashkani, Synthesis, characterization, and morphological control of Na ½ Bi ½

$Cu_3Ti_4O_{12}$ through modify sol–gel method. J. Mater. Sci.: Mater. Electron. **26**, 4848–4853 (2015)
35. S.S. Mali, H. Kim, C. Shim, P.S. Patil, J.H. Hong, C.K. Kim, Surfactant free most probable TiO_2 nanostructures via hydrothermal and its dye sensitized solar cell properties. Sci. Rep. **3**, 3004 (2013)
36. E. Hosono, S. Fujihara, K. Kakiuchi, H. Imai, Growth of submicrometer-scale rectangular parallelepiped rutile TiO_2 films in aqueous $TiCl_3$ solutions under hydrothermal conditions. J. Am. Chem. Soc. **126**, 7790–7791 (2004)
37. N. Bai, S. Li, H. Chen, W. Pang, Preparation, characterization and photoluminescence properties of mesolamellar titanium dioxide films. J. Mater. Chem. **11**, 3099–3102 (2001)
38. A. Sobhani-Nasab, S. Hosseinpour-Mashkani, M. Salavati-Niasari, H. Taqriri, S. Bagheri, K. Saberyan, Synthesis, characterization, and photovoltaic application of $NiTiO_3$ nanostructures via two-step sol–gel method. J. Mater. Sci.: Mater. Electron. **26**, 5735–5742 (2015)
39. L. Chu, Z. Qin, Q. Zhang, W. Chen, J. Yang, X. Li, Mesoporous anatase TiO_2 microspheres with interconnected nanoparticles delivering enhanced dye-loading and charge transport for efficient dye-sensitized solar cells. Appl. Surf. Sci. **360**, 634–640 (2016)
40. C. Huang, Y. Hsu, J. Chen, V. Suryanarayanan, K. Leeb, K. Ho, The effects of hydrothermal temperature and thickness of TiO_2 film on the performance of a dye-sensitized solar cell. Sol. Energy Mater. Sol. Cells **90**, 2391–2397 (2006)